SSRG International Journal of Electrical and Electronics Engineering
ISSN: 2348-8379/ https://doi.org/10.14445/23488379/IJEEE-V10I5P120

Volume 10 Issue 5, 213-226, May 2023

Original Article

Free Body Diagram Analysis and Finite Element Method Analysis of Wall Climbing Robot using the Hybrid Adhesive Mechanism

Rakesh Rajendran[1], Joshuva Arockia Dhanraj[2]

[1, 2]*Centre for Automation and Robotics (ANRO), Department of Mechatronics Engineering, Hindustan Institute of Technology and Science, Padur, Chennai, Tamil Nadu, India*

[1]*Corresponding Author : rakeshassistantprofessor@gmail.com*

Received: 20 March 2023 Revised: 29 April 2023 Accepted: 19 May 2023 Published: 31 May 2023

Abstract *- Many innovative approaches have been proposed in modelling and designing the wall climbing robot. Among all these approaches, the main focus is the adhesive mechanism of a wall climbing robot (WCR). This adhesive mechanism is a critical design consideration feature when discussing system reliability. There are various types of adhesive mechanisms like magnetic, suction cup, vacuum, rope and rail, electrostatic, fusion or hybrid type etc., of which the fusion or hybrid mechanism is found to have more payload to weight ratio (P/W value). This paper proposes a hybrid method using both permanent magnet (Nd FeB magnetic wheel) and solenoid electromagnet suction at the central disc. The design is validated using a free-body diagram, and its magnetic adhesion is analyzed by visualizing the magnetic flux density lines through Finite Element Method Magnetics (FEMM) analysis software. Three different analyses in FEMM are made, and their corresponding outcome is discussed concerning its graph.*

Keywords *- Finite Element Method Magnetics (FEMM), Nd FeB magnetic wheel, Payload to weight ratio.*

1. Introduction

The free-body diagram of the proposed design is drawn, and its corresponding adsorption force equation is derived as proposed by Zhang et al. [1]. The proposed design is further subjected to the simulation study on the flow of magnetic flux lines. The magnetic flux density analysis is done under three different methodologies, elaborated in detail with the flow chart fig [5,8,13] below.

2. Literature Survey

Liu et al. [2] proposed a 1D Halbach magnet array, and they tested its performance by analyzing magnetic flux density and air gap analysis using FEM. In contradiction, Sim et al. [3] proposed the AB method as an alternative to the FEM method to analyze the performance of the same Halbach array. Similarly, Noh et al. [4] proposed an analytic force model for finding the flux density that prevails in the gap between the wheel and surface and the results were compared with the analysis via FEM. Liu et al. [5] proposed using another software Ansoft-Maxwell to measure the bot's performance.

Howlader et al. [6] used a free-body diagram and finite element analysis method to justify the proposed wall climbing robot design. Joo et al. [7] proposed another WCR using a free body diagram and an ansoft-maxwell analysis to determine the magnetic flux density flow. Wang et al. [8] proposed using a free-body diagram and Ansys software for FEA analysis. YADAV et al. [9-11] used FEMM and Ansys Maxwell to design and validate the bot's performance. Ordoñez et al. [12] proposed an electromagnetic vibration energy harvesting method for cylindrical magnets which was further analyzed using FEMM.

Salloom et al. [13] developed magneto-rheological valves, and their performance is studied using FEMM software. Zhang et al. [14, 15] used FEMM to analyze the variation in magnetic flux density concerning air gap and free body diagram for both static and dynamic analysis of the bot. Tokhi et al. [16, 17] proposed magnetic adhesive for concrete walls, and the design was validated with Ansys FEM software.

Faisal et al. [18, 19] used a free-body diagram showing the suction mechanism used in the bot. Shang et al. [20, 21] proposed FEM analysis for electromagnetic suction. Cardenas et al. [22] proposed an electro-permanent magnet wheel and studied its behaviour using simulation software. Yan et al. [23] presented how to construct and study magnetic fields using FEMM software.

2.1. Free Body Diagram

2.1.1. Case 1

The wall-climbing robot is analyzed in the static mode under case 1, and by visualizing the force acting on the body as shown in Fig 1, equation 1.1 has arrived. In this state, the wall-climbing robot will be parallel to the ground. Where the adhesive force that exerts from each wheel is denoted as Xi, the weight of the whole robot is denoted as Wg and the desired adsorption force is denoted as F_a^1.

$$\sum_{i=1}^{4} Xi + \sum_{i=0}^{3} Yi = W_g + F_a^1 \quad (1)$$

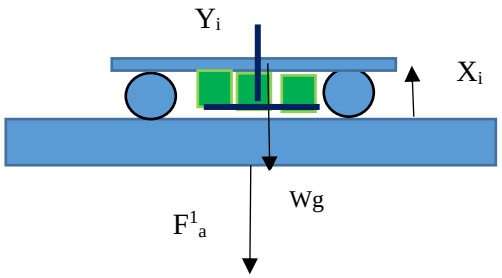

Fig. 1 Force acting when the bot is in horizontal

2.1.2. Case 2

The force acting on the WCR under case 2 can be visualized, as shown in Fig 2. In this state, the most likely mishap scenario of the wall-climbing robot is that it will slide down and roll over. The desired adsorption force (F2a) must fulfil the following equation (1.2) to avoid this mishap.

$$\sum_{i=1}^{4} Xi + \sum_{i=0}^{3} Yi = W_g \cos\theta + F_a^2 \quad (2)$$

$$F_{fric}^2 = \sum_{i=1}^{4} fi + \sum_{d=0}^{3} fd$$

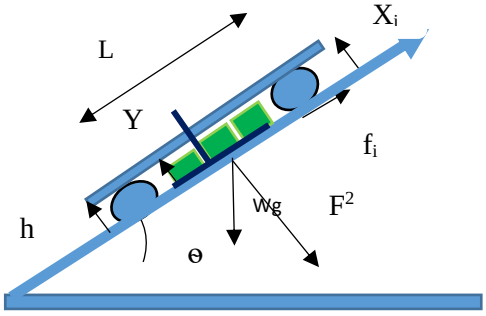

Fig. 2 Force acting when the bot is in inclined to angle ɵ

Where Xi is the adhesive force on each wheel, W_g represents the weight of the bot, and the desired adsorption force is denoted by F_a^2, the angle between the robot and the horizontal plane is denoted by θ, the friction force on each wheel is denoted as fi, the electromagnetic friction force exerted from the central disc is denoted as fd, and the resulting force of friction is denoted as F_{fric}^2

2.1.3. Case 3

In case 3, the force acting on the WCR can be visualized, as shown in Fig 3. The most likely mishap in this state is that the robot disentangles along the expected direction. The adsorption force (F_a^3) must fulfil the following equation (1.3) to avoid any mishap.

Where the adhesive force on each wheel is denoted as Xi, the weight of the whole robot is denoted as W_g and the desired adsorption force is denoted as F_a^3.

$$F_a^3 = W_g + \sum_{i=1}^{4} Xi + \sum_{i=0}^{3} Yi \quad (3)$$

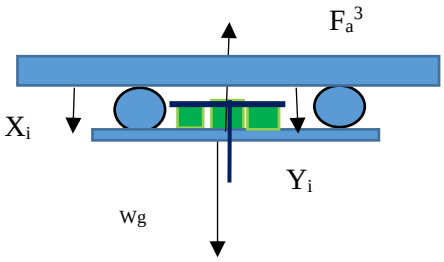

Fig. 3 Force acting when the bot is in tilted upside down

2.1.4. Case 4

In case 4, the analysis of the force of the wall-climbing robot can be simplified, as shown in Fig 4. In this state, the possible mishap for the robot is to roll over. The adsorption force must fulfil the following equation (1.4) to avoid this mishap. The adhesive force on each wheel is denoted as Xi, and the weight of the whole robot is denoted as W_g, the desired adsorption force is denoted as F_a^4 and fi represents the friction force on each wheel, and fd represents the frictional force exerted by the electromagnet at the central disc.

$$W_g = \sum_{i=0}^{4} fi + \sum_{d=0}^{3} fd$$

$$F_a^4 = \sum_{i=1}^{4} Xi + \sum_{i=0}^{3} Yi \quad (4)$$

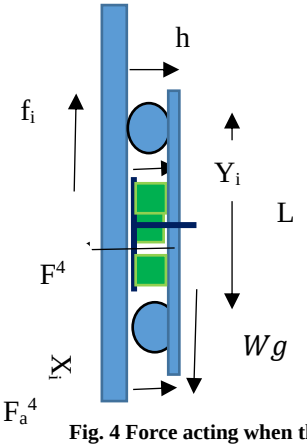

Fig. 4 Force acting when the bot is on a vertical wall

Considering the weight(G) of the bot as 3.5 kg, which is equal to approximately 34 N, each magnetic wheel (NdFeB) exerts 330 N (the count of the magnetic wheel is varied by varying X value), and each solenoid magnetic suction cup exerts 147 N (the count of the Solenoid is varied by varying the Y value) and finding the adhesive force (F_a) value for each case by substituting the values in the equations a, b, c and d. The below Table1 shows the consolidated value of Fa in all cases Below, Table 2 shows the comparison of Fa values for all the cases

Table 1. Fa versus no: of electromagnet at central disc

Central Disc Solenoid Count (Y)	Y=0	Y=1	Y=2	Y=3
Case 1	1286 N	1433 N	1580 N	1727 N
Case 2 Considering	1296 N	1443 N	1590 N	1737 N
Case 3	1354 N	1501 N	1648 N	1795 N
Case 4	1320 N	1467 N	1614 N	1761 N

Table 2. Comparison of F_a value for all 4 cases

Case	Adhesive Force Value (N)	Payload Capacity(kg-f)	Max (F1, F2, F3, F4)
1	1727	176	1795
2	1737	177	
3	1795	183	
4	1761	179.5	

From the free body diagram, the payload capacity should be 0 to 183 kg-f, but practically speaking, the maximum adhesive force exerted will be 179.5kg-f. Hence while considering case 3 (upside down position, considering the bot's weight as 34N (along with payload capacity), the bot will be allowed to have a maximum payload of 176 kg-f. Hence, the proposed system has a maximum adhesive force of 1761N and a payload capacity range between 0 - 179.5 kg-f, which is better suitable for high payload applications.

3. Software

Though there are software like Anysis, Ansoft-maxwell for performing finite element analysis, the FEMM software has multiple features for analysis. This paper uses FEMM analysis software to validate and justify the proposed design concerning the flow of magnetic flux lines. It is essential to analyze whether the magnetic flux lines are uniformly distributed throughout the length of the wall climbing robot, ensuring the bot's stability and even avoiding the peel-off or slippage effect. The wall climbing robot is of length 30 cm. The B-H curve value has to be given as input for the core, the current density value has to be as input to the solenoid windings. After declaring the boundary and before creating the mesh, ensure that all the materials are declared for the blocks, now analyze and view the result with a flux density plot. The current density J= NI/L. Considering the length of the wire (L) as 280mm and the diameter of the wire (G_w) as 1.2 mm, the number of turns N = L/$G_{w\ equals}$ 233.33. Now substituting the value as 233.33 for N to find the current density. Considering the operating current, I as 300 mA and the surface current density (J_s).

$$J_s = \frac{NxI}{L} = \frac{233.33x300}{280} = 250$$

By applying the value, we get the current density value as 250. The side view and top view of the proposed hybrid design is as shown in Fig. 14 & 15.

3.1. Case Analysis 1

The bot consists of magnetic wheels and solenoids placed on the bot's chassis. The count of the Solenoid is varied from 1,2, and 3. The magnetic flux line for each case is given below. It is seen that when we use three solenoids, we have more magnetic flux generated uniformly along the length of the robot. In case 1, the graph shows that the peak flux density appears only at the chassis centre where the electro-solenoid is placed. Considering case 2, the graph says there are two peaks positioned at two ends of the length of the bot. In case 3, the flux density and the bot's length are uniform. This is very much needed for producing stability on wall-climbing robots. The detailed methodology of this analysis is given in the flowchart, as shown in Fig 5. The magnetic flux density and plot are given in Fig 6 and 7, respectively.

3.2. Case Analysis 2

Now the air gap between the chassis and electromagnet is varied to check the magnetic flux line distribution by varying the electromagnet count at the central disc. The air gap is 0.5 cm,1.0 cm and 1.5cm between the chassis and the vertical wall. In case 1, when there is a minimum air gap (i.e. 0.5 cm), the magnetic flux density value is maximum, and the peak overshoot value is around 2.4 tesla. In this case 1, the mean value of the magnetic flux density is greater than the other two cases (i.e. 1.0 cm and 1.5 cm). Considering the second case (1.0 cm), the peak overshoot value lies around 2.2 tesla, and the mean value of the magnetic flux density is not up to that of case 1. Case 3 has the air gap as 1.5cm, and the analysis shows the peak overshoot value as 1.9 tesla and the mean value of the flux density is less The detailed methodology of this analysis is given in the flowchart as shown in Fig 8. The magnetic flux density and plot are given in Fig 9 and 10, respectively.

3.3. Case Analysis 3

Now the thickness of the wall is varied, and the analysis is done in three different cases. In the first case, the wall thickness is considered to be 0.5 cm, and magnetic flux lines are found to be penetrating the wall. It shows that the overall thickness of the wall is influenced by magnetic flux lines that

emerged from both magnetic wheels and electromagnetic solenoids used at the central disc. The peak overshoot value, in this case, has reached 2.6 tesla. The second case has a wall thickness of 1 cm, and the analysis shows that magnetic flux lines are being penetrated. However, the peak overshoot value is 2.4 tesla and the mean value of magnetic flux density less than that of case 1. In case 3, the wall thickness is 1.5 cm, the peak overshoot value, in this case, is 2.2 tesla, and the mean value of the magnetic flux density would be less than in the other two cases. The detailed methodology of this analysis is given in the flowchart, as shown in Fig 11. The magnetic flux density and plot are given in Fig 12 and 13, respectively.

4. Illustration

The study reveals that the proposed wall climbing robot design performs better when compared to the existing one. Noh et al. [4] have mentioned that 0.8T magnetic flux is exerted with an air gap of 0.8 mm, whereas the proposed system exerts magnetic flux in the range of 2T for the same air gap distance. The proposed wall climbing robot design has a higher magnetic flux density value with a surface thickness of 10mm when compared to the one designed by Yadav et al. [9]

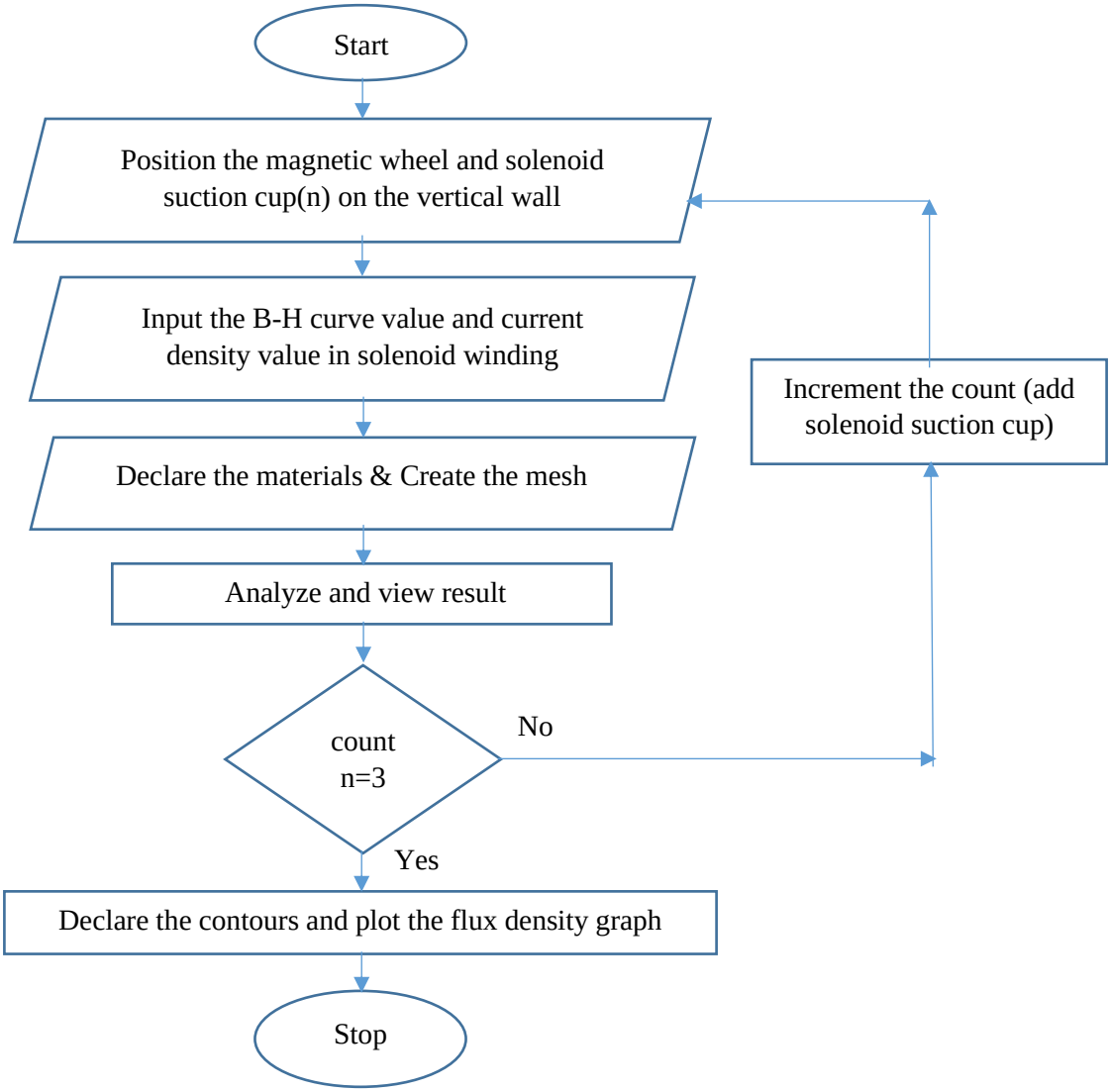

Fig. 5 Flow chart methodology in FEMM analysis – varying the count of central electro magnets contacting the surface

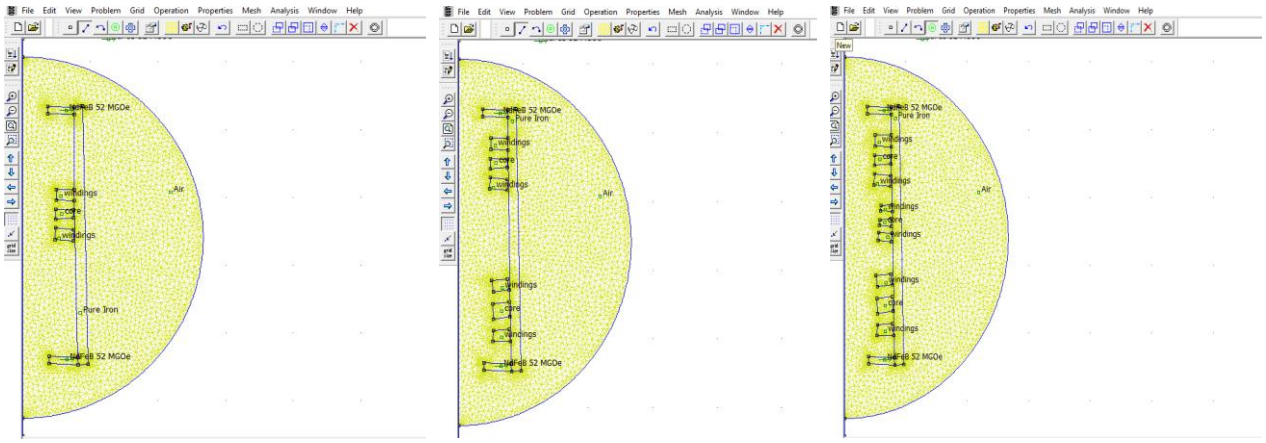

FEMM Result- Magnetic Flux lines

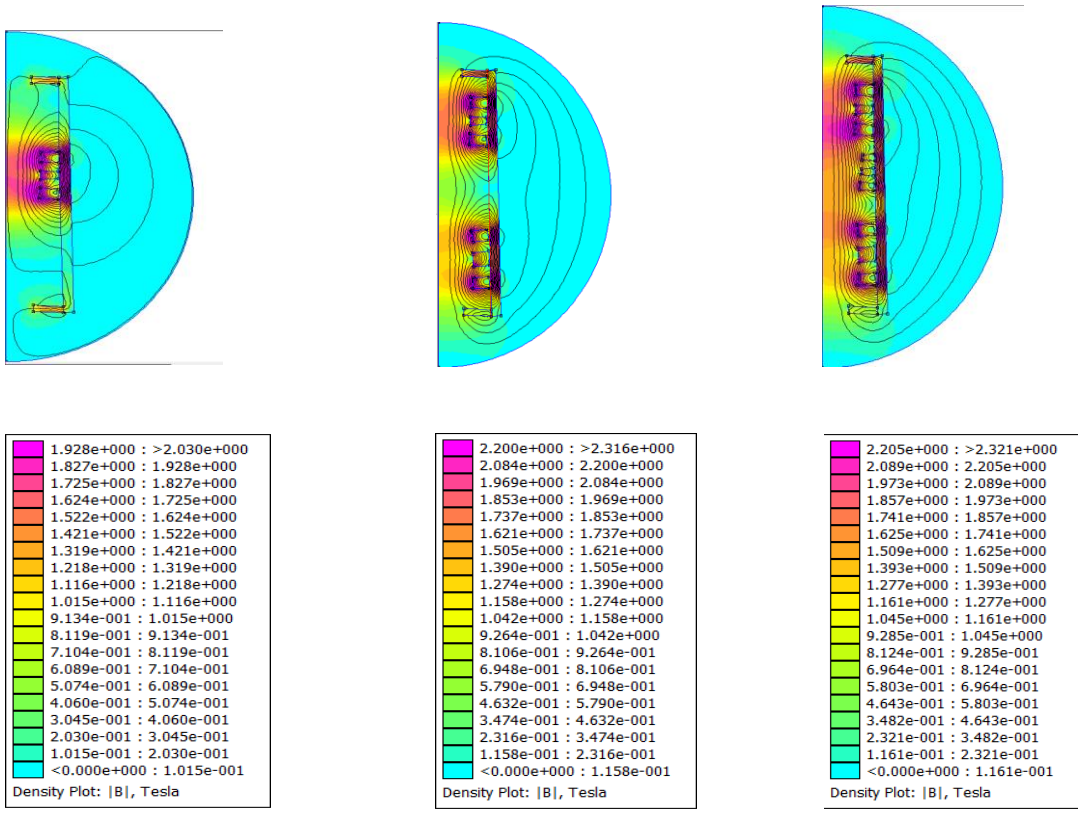

Fig. 6 FEMM analysis – varying the count of central electro magnets on surface

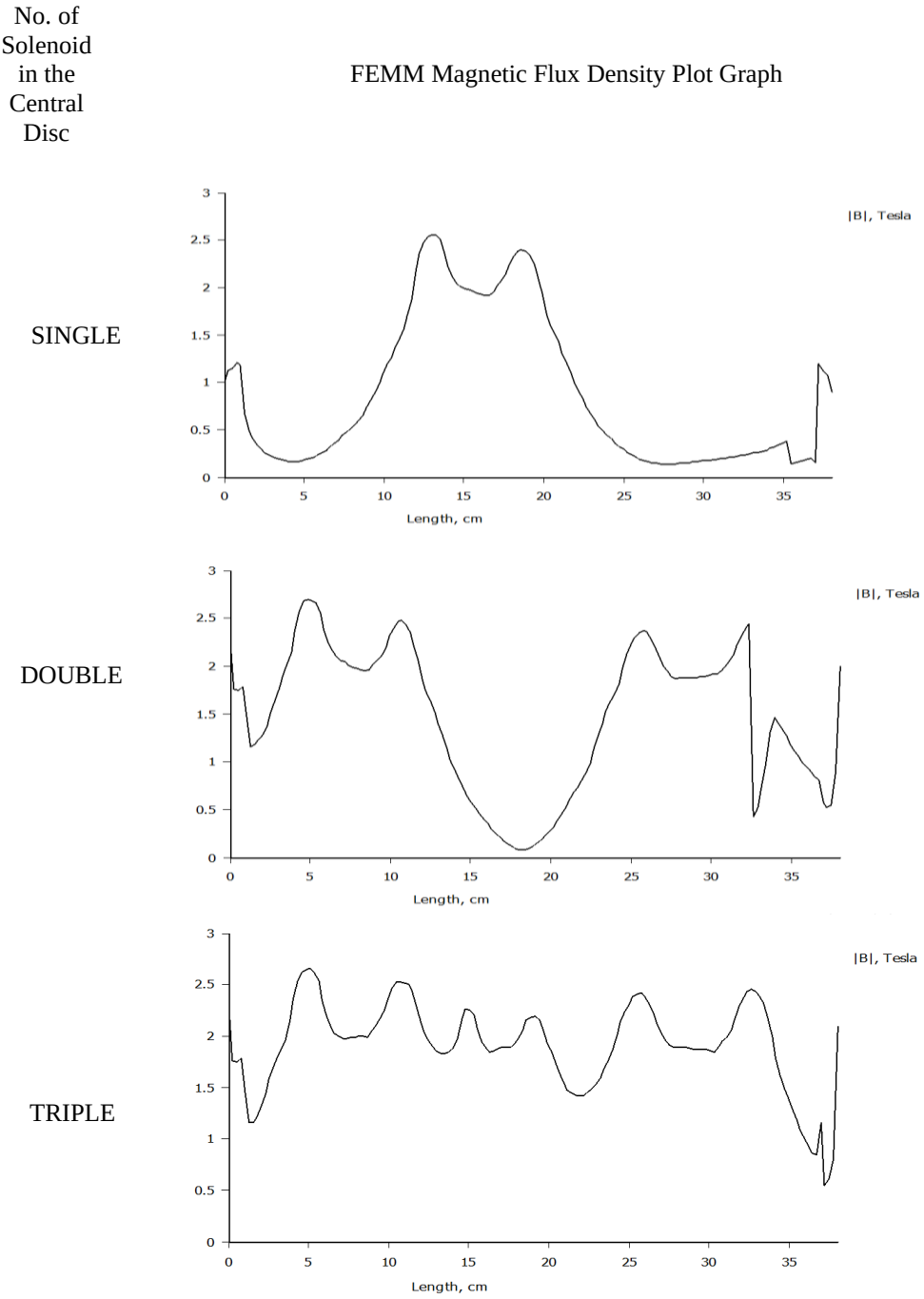

Fig. 7 Output of FEMM analysis – varying the count of central electro magnets

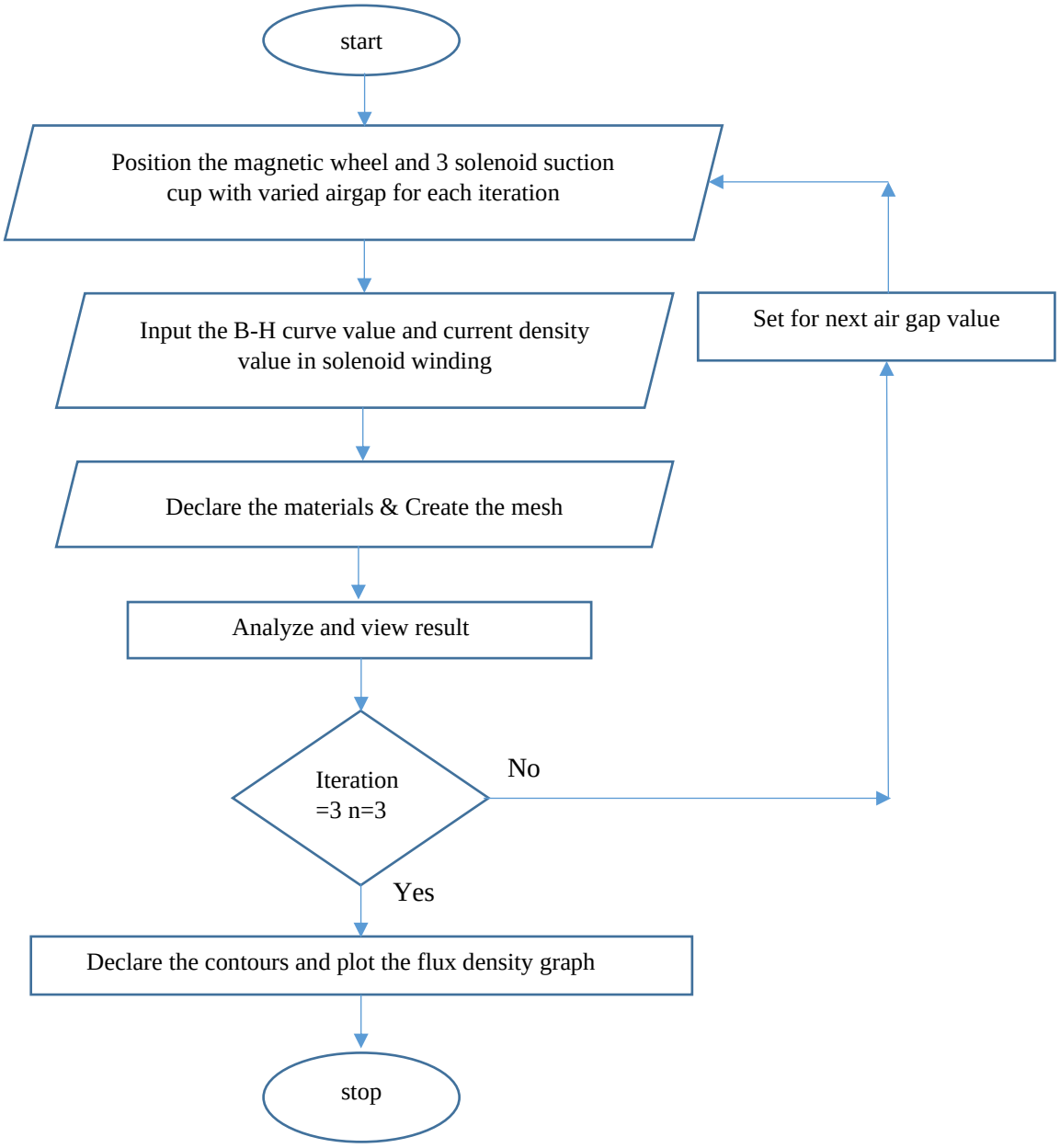

Fig. 8 Flow chart methodology in FEMM analysis – varying air gap (standoff distance)

S.No	0.5 CM AIR GAP	1.0 CM AIR GAP	1.5 cm air gap
1	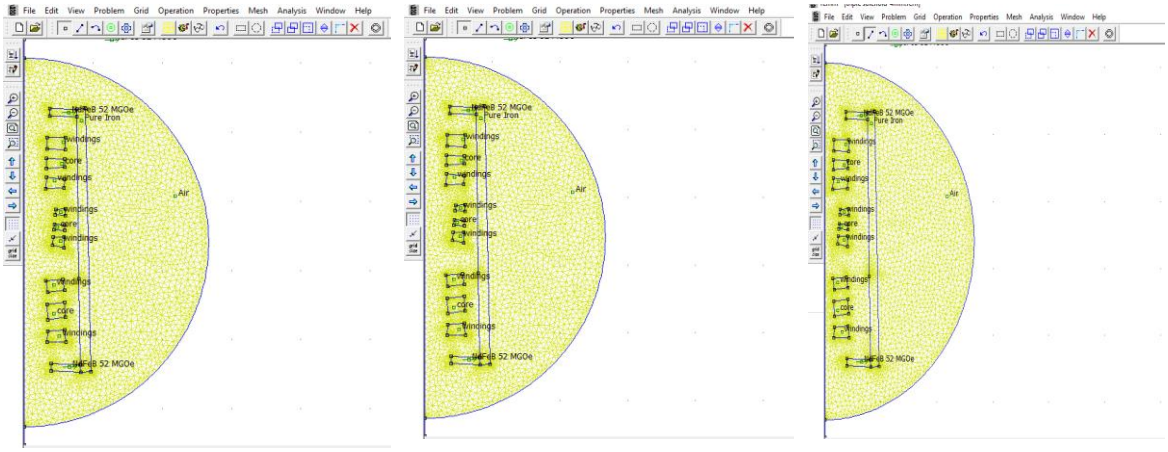		
2	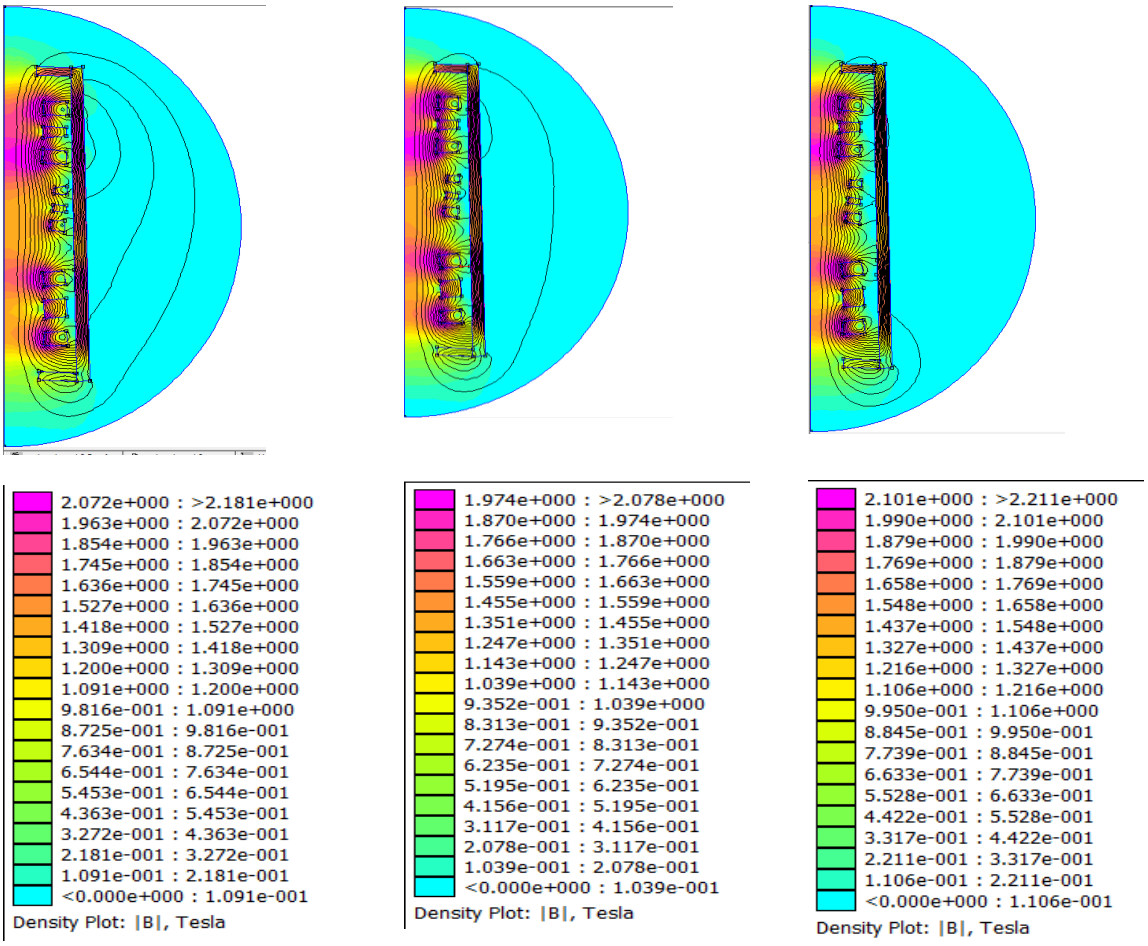		

Fig. 9 FEMM analysis – varying air gap (standoff distance)

Air gap (cm)	Graph
Case 1: Air gap 0.5 cm	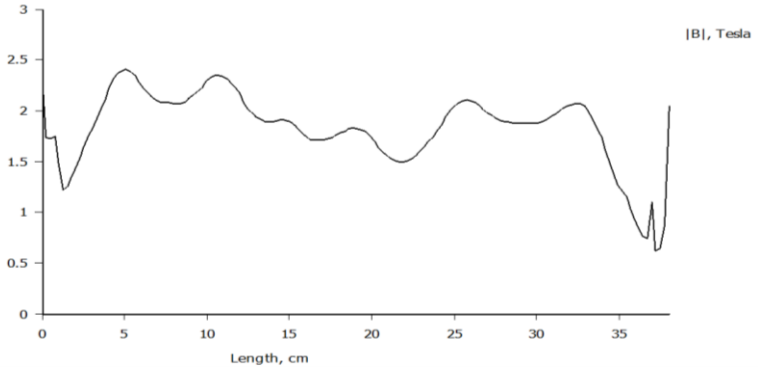
Case 2: Air gap 1.0 cm	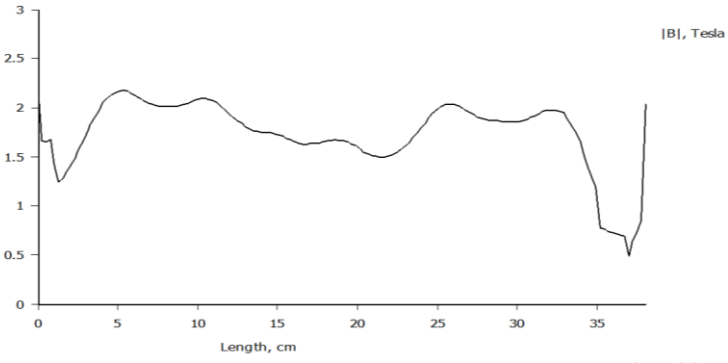
Case 3: Air gap 1.5 cm	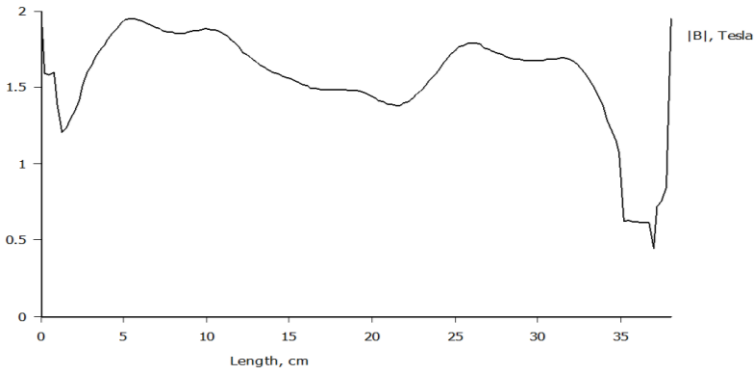

Fig. 10 Output of FEMM analysis – varying air gap (standoff distance)

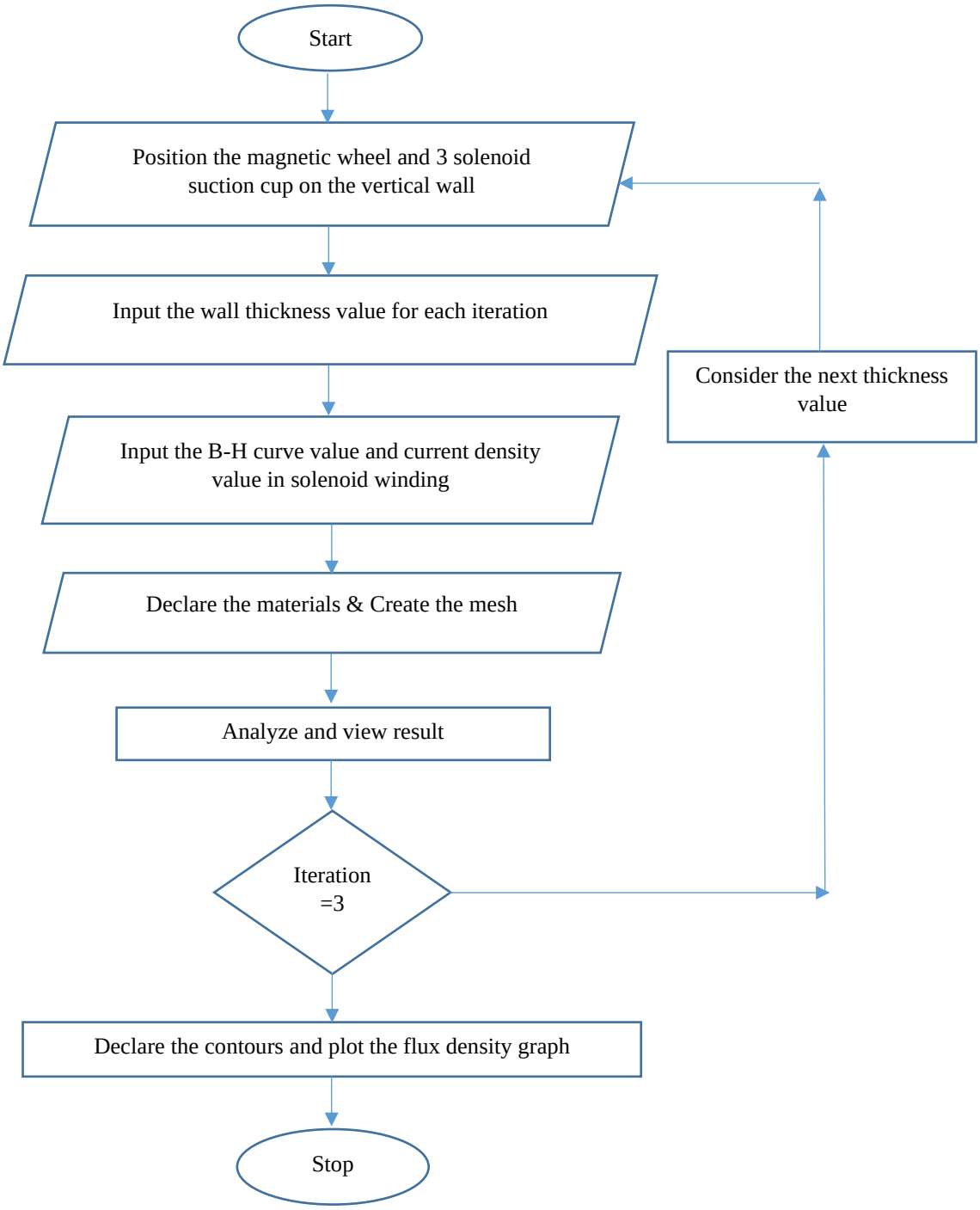

Fig. 11 Flow chart methodology in FEMM analysis – varying wall thickness

S.No	0.5 CM thickness	1 CM thickness	1.5 cm thickness
1	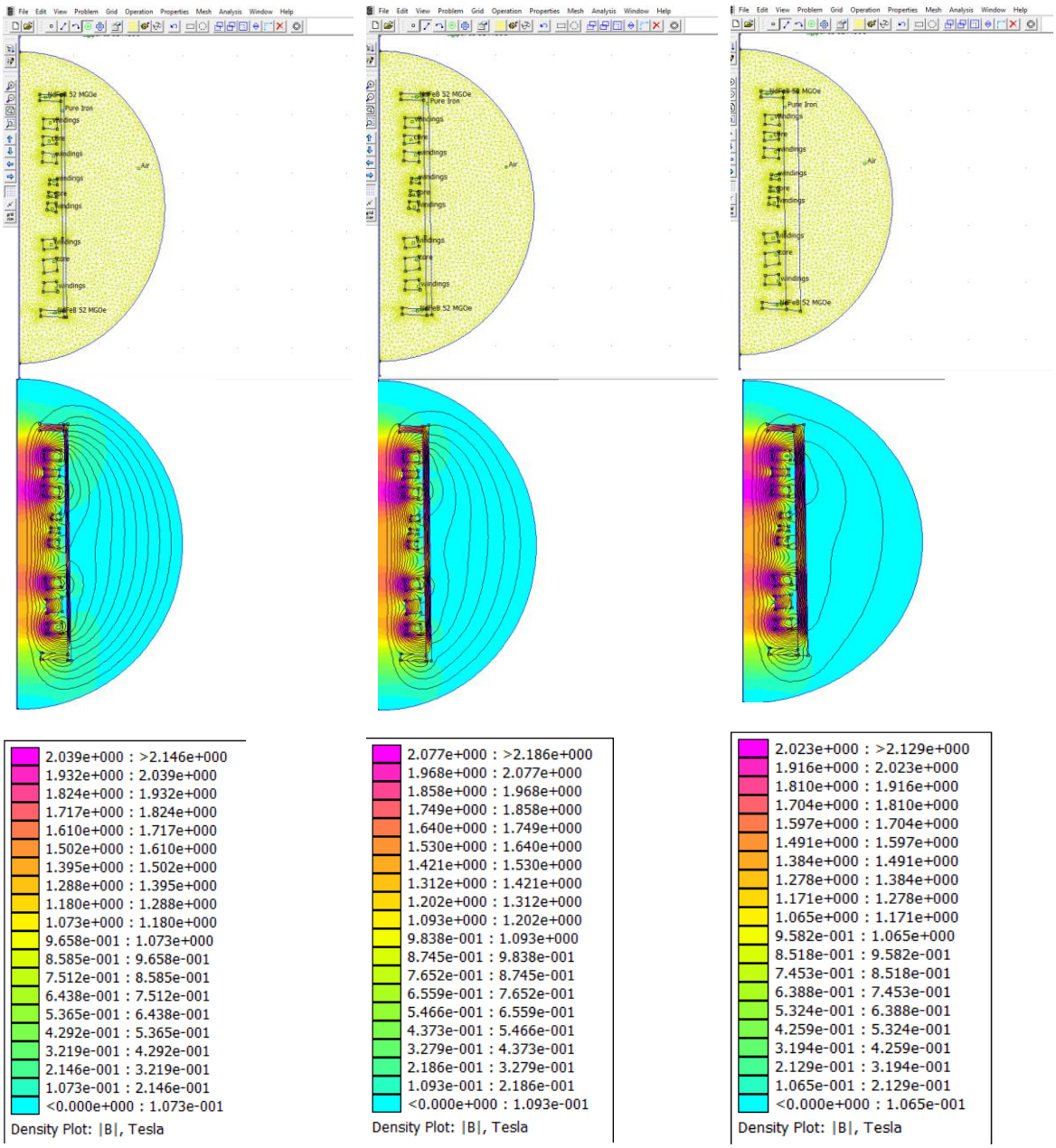		
2			

Fig. 12 FEMM analysis – varying wall thickness

The thickness of the wall (cm)	Graph
Case1: Wall thickness: 0.5 cm	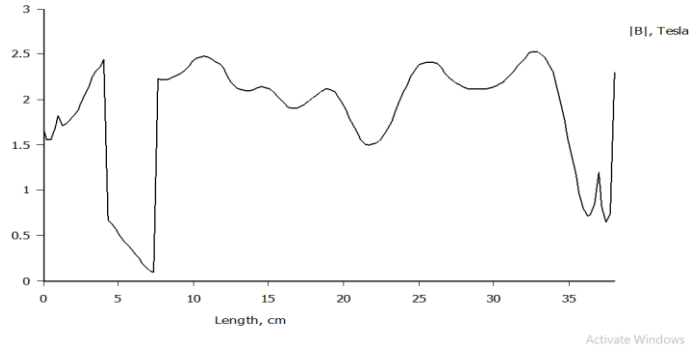
Case 2: Wall thickness: 1 cm	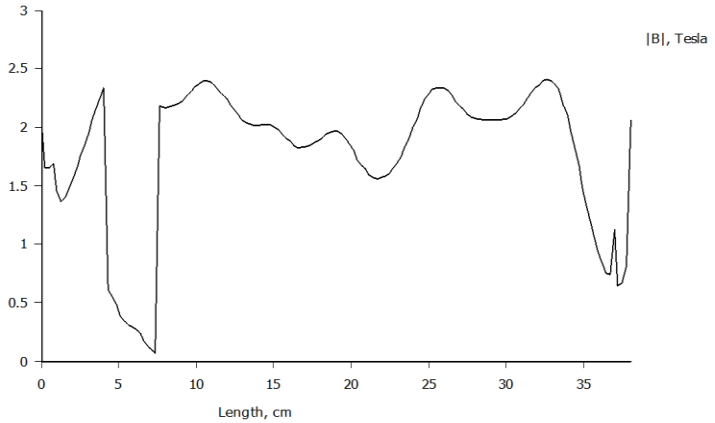
Case 3: Wall thickness: 1.5 cm	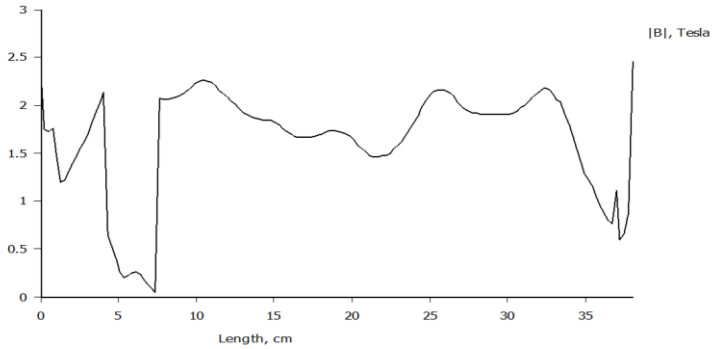

Fig. 13 Output of FEMM analysis – varying wall thickness

Table 3. Comparison of the magnetic flux density value with existing vs proposed design

S.No	Parameter	Noh et al. [4]	Proposed	Yadav et al. [9]	Proposed
1	Air gap Vs Tesla	Airgap=0.8 Tesla=0.8 T	Air gap =0.8 Tesla ≅2 T	-	-
2	Magnetic flux density value with a Surface thickness 10 mm	-	-	$1.012e^{00}$:>$1.065e^{00}$	2.07 e^{00}: >2.18 e^{00}

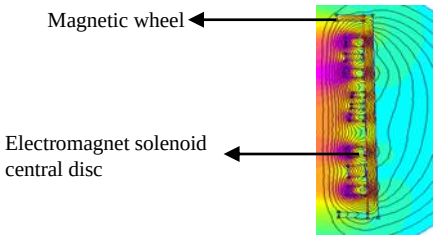

Fig. 14 Side view

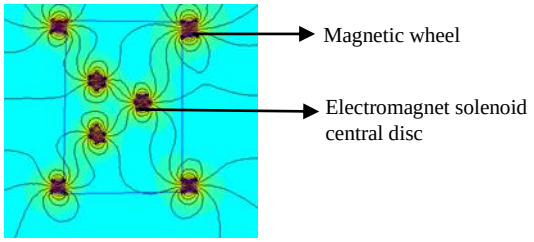

Fig. 15 Top view of the WCR

5. Conclusion

Finally, the maximum adhesive force (1727 to 1761 N) is exerted by using three solenoids at the central disc using free body diagram analysis, and when we extend the study using FEMM software under three different case analyses, the same three electromagnet solenoids at the central disc perform much better in all three analyses.

The proposed hybrid design having three electromagnets at the central disc and four permanent magnetic wheels, performs much better while considering adhesion and magnetic flux density distribution throughout the length of the bot. The study also reveals the minimum standoff distance (air gap) and wall thickness required for better performance.

References

[1] Yulong Zhang et al., "A Novel Magnetic Circuit Design Method for a Permanent Magnetic Chuck of a Wall-Climbing Robot," *Energies*, vol. 15, no. 18, pp. 1-17, 2022. [CrossRef] [Google Scholar] [Publisher Link]

[2] Guangdou Liu et al., "Design of a New 1D Halbach Magnet Array with Good Sinusoidal Magnetic Field by Analyzing the Curved Surface," *Sensors*, vol. 21, no. 7, pp. 1-17, 2021. [CrossRef] [Google Scholar] [Publisher Link]

[3] Min-Seob Sim, and Jong-Suk Ro, "Semi-analytical Modelling and Analysis of Halbach Array," *Energies*, vol. 13, no. 5, pp. 1-11, 2020. [CrossRef] [Google Scholar] [Publisher Link]

[4] Myounggyu Noh et al., "Modeling of Attractive Force by Magnetic Wheel used for a Mobile Robot," *Actuators*, vol. 9, no. 3, pp. 1-9, 2020. [CrossRef] [Google Scholar] [Publisher Link]

[5] Jun Liu et al., "Development of a New Type of Automatic Magnetic Particle Inspection Wall-climbing Robot," *Advances in Mechanical Engineering*, vol. 13, no. 9, pp. 1-15, 2021. [CrossRef] [Google Scholar] [Publisher Link]

[6] Howlader, MDOF, and Sattar, T. P., "Finite Element Analysis-based Optimization of Magnetic Adhesion Module for Concrete Wall Climbing Robot," *International Journal of Advanced Computer Science and Applications*, vol. 6, no. 8, pp.8-18, 2015. [CrossRef] [Google Scholar] [Publisher Link]

[7] Jae Young Joo, and Yeon Taek Oh, "Study of Wall Climbing Robot Having Proposition of Stable Mechanism on the Inclined Plane Based on Magnetic Force," *Journal of Automation and Control Engineering*, vol. 7, no. 1, 2019. [CrossRef] [Google Scholar] [Publisher Link]

[8] Yang Wang et al., "Self-compliant Track-type Wall-climbing Robot for Variable Curvature Façade," *IEEE Access*, vol. 10, pp. 51951-51963, 2021. [CrossRef] [Google Scholar] [Publisher Link]

[9] Arun Kumar Yadav, and Janusz Szpytko, "Magnetic Wheeled Automated Robot for Structural Health Monitoring of Overhead Cranes by using NDT Method," *3rd Singapore International Non-destructive Testing Conference and Exhibition (SINCE2019)*, 2019. [Google Scholar] [Publisher Link]

[10] Sachin Komble et al., "Fire Fighting Robot," *International Journal of Recent Engineering Science*, vol. 10, no. 2, pp. 54-60, 2023. [CrossRef] [Publisher Link]

[11] Ordóñez Izquierdo et al., "Analysis of Different Cylindrical Magnet and Coil Configurations for Electromagnetic Vibration Energy Harvesters," *Periodicals of Engineering and Natural Sciences*, vol. 9, no. 2, pp. 1055-1063, 2021. [CrossRef] [Google Scholar] [Publisher Link]

[12] Maher Yahya Salloom, "FEM Analysis and Design of Permanent Magnet Disk Type Magneto-rheological (MR) Valve," *AIP Conference Proceedings*, vol. 2213, no. 1, 2020. [CrossRef] [Google Scholar] [Publisher Link]

[13] Minglu Zhang et al., "Optimization Design and Flexible Detection Method of a Surface Adaptation Wall-Climbing Robot with Multisensor Integration for Petrochemical Tanks," *Sensors*, vol. 20, no. 22, pp. 1-20, 2020. [CrossRef] [Google Scholar] [Publisher Link]

[14] HaoLi et al., "The Blind Corner Intelligent Cleaning Assistant Based On Sweeping Robot," *International Journal of Computer and Organization Trends*, vol. 11, no. 3, pp. 1-4, 2021. [CrossRef] [Publisher Link]

[15] Tokhi, M. O., and Sattar, T. P., "Design and Parametric Investigations of Permanent Magnet Adhesion Mechanism for Robots Climbing on Reinforced Concrete Walls," *CLAWAR 2020: 23rd International Conference on Climbing and Walking Robots and the Support Technologies for Mobile Machines*, 2020. [Google Scholar] [Publisher Link]

[16] Zhang Huanyu et al., "Design of a Three-in-One Bionic Chameleon Robot," *International Journal of Computer and Organization Trends*, vol. 13, no. 1, pp. 13-15, 2023. [CrossRef] [Publisher Link]

[17] Riad Hossain Faisal, and Nafiz Ahmed Chisty, "Design and Implementation of a Wall Climbing Robot," *International Journal of Computer Applications*, vol. 179, no. 13, pp.1-5, 2018. [Google Scholar] [Publisher Link]

[18] Harpreet Singh, Naveen Dhillon, and Kailash Rawat, "ANFIS Based Forward and Inverse Kinematics of Six Arm Robot Manipulator with Six Degree of Freedom," *International Journal of Computer & Organization Trends (IJCOT)*, vol. 5, no. 2, pp. 49-54, 2015. [CrossRef] [Publisher Link]

[19] Weiyan Shang, Canjun Yang, and Faju Qiu, "Design and Analysis of Four-Legged Wall-Climbing Robot," *Academic Journal of Manufacturing Engineering*, vol. 17, no. 2, 2019. [Google Scholar] [Publisher Link]

[20] Yeon Taek OH, "Study of Wall Climbing Robot through the Simulation of Multi-Body Dynamics," *International Journal of Engineering Trends and Technology*, vol. 70, no. 11, pp. 138-143, 2022. [CrossRef] [Publisher Link]

[21] Francisco Ochoa-Cardenas, and Tony J. Dodd, "Design of an Active Magnetic Wheel with a Varying Electro-Permanent Magnet Adhesion Mechanism," *2015 IEEE/RSJ International Conference on Intelligent Robots and Systems (IROS)*, 2015. [CrossRef] [Google Scholar] [Publisher Link]

[22] N. Navaprakash, Uppu Ramachandraiah, and G. Muthukumaran, "Information Based Remote Control System for Climbing Robot Applications," *International Journal of Engineering Trends and Technology*, vol. 68, no. 3, pp. 6-11, 2020. [Publisher Link]

[23] Rongguo Yan et al., "Design and Analysis of a Magnetic Connection Device for the External Ventricular Drain," *IET Science, Measurement & Technology*, vol. 17, no. 2, pp. 84-92, 2023. [CrossRef] [Google Scholar] [Publisher Link]